Insolation and glacial-interglacial control on southwestern African hydroclimate over the past 140,000 years

James A. Collins[1,*], Enno Schefuß[1], Aline Govin[1], Stefan Mulitza[1], Ralf Tiedemann[2]

1) MARUM – Center for Marine Environmental Sciences, University of Bremen, D-28359 Bremen, Germany

2) Alfred Wegener Institute for Polar and Marine Research, Am Alten Hafen 26, D-27568 Bremerhaven, Germany

* Now at: Alfred Wegener Institute for Polar and Marine Research, Am Alten Hafen 26, D-27568 Bremerhaven, Germany

Email: jcollins@awi.de

Abstract

The past climate evolution of southwestern Africa is poorly understood and interpretations of past hydrological changes are sometimes contradictory. Here we present a record of leaf-wax δD and $\delta^{13}C$ taken from a marine sediment core at 23°S off the coast of Namibia to reconstruct the hydrology and C_3 versus C_4 vegetation of southwestern Africa over the last 140,000 years (140 ka). We find lower leaf-wax δD and higher $\delta^{13}C$ (more C_4 grasses), which we interpret to indicate wetter Southern Hemisphere (SH) summer conditions and increased seasonality, during SH insolation maxima relative to minima and during the last glacial period relative to the Holocene and the last interglacial period. Nonetheless, the dominance of C_4 grasses throughout the record indicates that the wet season remained brief and that this region has remained semi-arid. Our data suggest that past precipitation increases were derived from the tropics rather than from the winter westerlies. Comparison with a record from the Congo Basin indicates that hydroclimate in southwestern Africa has evolved in antiphase with that of Central Africa over the last 140 ka.

Keywords: Leaf-wax n-alkane, Hydrogen and carbon isotopes, African palaeoclimate, monsoonal precipitation, Namibia

1. Introduction

Tropical to sub-tropical southwestern Africa (between about 17°S and 30°S) experiences semi-arid to hyper-arid conditions (Tyson, 1986) due its position in-between the influence of precipitation from low-latitude tropical climate systems in the north and mid-latitude climate systems in the south. It hence provides an important test-region for investigating past changes in the spatial distribution of these climate systems. Unfortunately, due to this aridity, long terrestrial palaeoclimate records are rare and thus our understanding of past changes in precipitation remains incomplete.

There is presently debate regarding the behavior of hydroclimate in southwestern Africa in response to the precessional (19-23 kyr cycle) insolation variations. Increased local summer insolation is expected to increase the land-ocean pressure gradient, bringing more warm, moist air on land and increasing precipitation delivered by the summer monsoon, as has been shown in the northern hemisphere (NH; e.g. Pokras and Mix, 1985; Rossignol-Strick, 1985). In line with this, a 200 ka long sedimentological record from Lake Tswaing in southeastern Africa, suggests that precipitation increased during precessional southern hemisphere (SH) summer insolation maxima (Partridge et al., 1997), due to an enhancement of the SH summer East African Monsoon. Similarly, a leaf-wax hydrogen isotope record from the Zambezi River (Schefuß et al., 2011) suggests relatively dry conditions during the mid-Holocene SH summer insolation minimum, relative to the deglacial and late Holocene. In contrast, a hyrax-midden record from the Namib Desert, spanning the last 11.7 ka, (i.e. one half of the last precessional cycle), suggests a progressive drying from the mid to late Holocene, i.e. wetter rather than drier conditions during the mid-Holocene SH summer insolation minimum (Chase et al., 2009). It was thus suggested that southwestern Africa responds in phase with northern hemisphere summer insolation (Chase et al., 2009). As such, on precessional timescales it is

not yet clear whether the hydrology of southwestern Africa is controlled by NH or SH summer insolation variations.

In addition to precessional insolation control, the effect of glacial versus interglacial boundary conditions on the hydroclimate of southwestern Africa is also under debate. For example, more desert and semi-desert vegetation during the last glacial period relative to the Holocene and last interglacial period (Shi et al., 2001; Collins et al., 2011) points to drier conditions during the last glacial period. In contrast, a marine grain-size record (Stuut et al., 2002) and a collection of terrestrial records (Chase and Meadows, 2006) suggest wetter conditions in southwestern Africa during the last glacial period, and depleted precipitation isotopes in precipitation would also point to wetter glacial conditions (Collins et al., 2013). Wetter glacial conditions in southwestern Africa have been interpreted to reflect a northward shift of the SH mid-latitude westerly wind belt during the last glacial period (Stuut et al., 2002, Chase and Meadows, 2006; Cockcroft et al., 1987). However, an alternative mechanism is a southward shift of tropical rain-producing systems due to the expanded NH ice sheets, as is commonly simulated by climate models (e.g. Kageyama et al., 2013). In summary, studies disagree whether southwestern Africa was wetter or drier during the last glacial period and, for those that do agree on the sign of the changes, different mechanisms have been invoked.

We investigate the effect of precessional insolation changes and glacial-interglacial boundary conditions on the climate of southwestern Africa using the hydrogen and carbon isotopic composition of terrestrial plant leaf-wax *n*-alkanes taken from a marine sediment core. *n*-Alkanes are straight chain hydrocarbon compounds produced as part of the protective layer on terrestrial plant leaves (Koch and Ensikat, 2008, Eglinton and Hamilton, 1967). The hydrogen isotopic composition (δD) of leaf wax *n*-alkanes is taken as a recorder of the hydrological history of precipitation (e.g. Sachse et al., 2012). The carbon isotopic composition ($\delta^{13}C$) of leaf-wax *n*-alkanes reflects the photosynthetic pathway of the plants i.e. the relative contribution of C_3 versus C_4 vegetation (e.g. Castañeda et al., 2009). We also assess the contribution of terrestrial inorganic material from XRF-major element analysis. Our sediment core is located off the coast of Namibia at 23°S and receives

terrestrial material mainly as dust from southwestern Africa. The sediment core extends back to 140 ka, covering six precessional cycles and allowing us to determine the control of NH or SH summer insolation on southwestern African climate. This time span also allows us test the effect of glacial boundary conditions during the last glacial period (Marine Isotope Stages; MIS 5.4 to MIS 2) on climate by comparison with two interglacial periods; the Holocene (MIS 1; from 10 ka to the present) and the last interglacial period (MIS 5.5; between 130 ka and 116 ka; Kukla et al., 2002). Finally, in order to understand regional-scale shifts in precipitation distribution, we compare our findings with other records from southwestern and tropical Central Africa.

2. Background and Regional Setting

2.1 Precipitation, moisture sources and controls on δD of precipitation

Southwestern Africa experiences arid conditions due to the South Atlantic Anticyclone, which is strongest and furthest south during SH winter (e.g. Tyson, 1986). The western part of Namibia experiences the most pronounced aridity due to the cold sea surface temperature of the Benguela upwelling region, which stabilises air and prevents convection (e.g. Eckardt et al., 2013 and references therein). Most precipitation delivered to southwestern Africa is tropical convective precipitation, which is delivered by the southernmost extension of the East African monsoon in SH summer (the northerly East African monsoon), resulting in decreasing precipitation amounts from NE to SW (**Fig 1a**). SH summer rainfall is associated with Tropical-Temperate Troughs (TTTs), the Congo Air Boundary (CAB) and the Angola Low (Eckardt et al., 2013). TTTs form when tropical systems connect with mid-latitude low pressure systems and form cloud bands which move eastward across southern Africa and are thought to be the most important source of moisture in southern Africa (Harrison, 1984; Todd et al., 2004). As well as tropical systems, the mid-latitude westerly winds bring a limited amount moisture to the very south of southwestern Africa when they shift northward during the SH winter season **(Fig. 1b)**. Finally, in the hyper-arid Namib Desert, fog constitutes a regular but minor source of moisture (Olivier, 1995). Most of the moisture delivered to southwestern Africa originates from the Indian Ocean (Gimeno et al., 2010; Rouault et al., 2003; Tyson, 1986). The

Atlantic Ocean also contributes some moisture to this region: to the north of the cold Benguela Upwelling, the SE tradewinds are deflected clockwise (e.g. Leroux, 1983, Servain and Legler, 1986), carrying some moisture on-land (e.g. Eckardt 2013; Rouault et al., 2003), and the winter westerlies also source moisture from the Atlantic Ocean (Rouault et al., 2003).

In the tropics, δD of precipitation (δD_p) is negatively correlated with precipitation amount, which is known as the amount effect (Dansgaard, 1964) and is evident in station data from southern Africa on seasonal to interannual timescales (IAEA/WMO, 2006). Two main mechanisms cause the isotopic depletion of precipitation: a) reduced re-evaporation of falling raindrops under a wetter atmosphere, and b) greater downdraughting of isotopically depleted vapour from high altitudes during stronger convection (Risi et al., 2008a). Because these processes control δD_p on timescales of a few days (Risi et al., 2008b), δD_p likely reflects the intensity of wet season precipitation, rather than the length of the wet season or overall amount of precipitation. In addition to local precipitation amount, non-local precipitation processes (e.g. Pausata et al., 2011) may be controlling δD_p in southwestern Africa. Thus, δD_p has also been interpreted as reflecting the intensity of the large-scale monsoon rather than local rainfall amount (Tierney et al., 2011). Lastly, δD_p can also controlled by moisture source. Due to greater rainout (continental effect) as air masses travel over land (e.g. Dansgaard, 1964; Rozanski et al., 1993), southwestern African moisture sourced from the Indian Ocean is more isotopically depleted than moisture sourced from the Atlantic Ocean. Thus, a relative increase in the proportion of Indian Ocean moisture would yield lower δD_p in southwestern Africa.

2.2 Sediment core and source areas of terrestrial material

To understand past climate in southwestern Africa, we investigated calypso core MD08-3167 (23°18.91'S; 12°22.61'E; **Fig. 1a**) which was retrieved from the continental slope off Namibia at 1948 m water depth during IMAGES cruise MD167/RETRO (Waelbroeck et al., 2008). Most of the clay material in marine sediments off the coast of Namibia today is illite, thought to be sourced as dust from the Namib Desert (Bremner and Willis, 1993). In terms of dust availability, the sand dunes and gravel plains which cover most of the Namib Desert are in a supply-limited state, due to prolonged

aridity and wind-erosion (Lancaster, 2002). However, dry ephemeral river beds and pans are major 'point-sources' of dust (Eckardt and Kuring, 2005). This dust is carried offshore by Bergwinds which blow perpendicular to the coast during SH autumn and winter (**Fig. 1b**; Eckardt and Kuring, 2005). Much of the catchment of the ephemeral rivers is located on the Namibian plateau (Fig. 1a; Eckardt and Kuring, 2005; Eckardt et al., 2013). Ephemeral rivers occasionally reach the ocean, delivering large amounts of sediment (Bremner and Willis, 1993) and recharging dust sources in the desert (Eckardt and Kuring, 2005). In addition to the point sources, the Makgadikgadi Basin in the Kalahari Desert and the Etosha Pan in Namibia have been identified as major dust sources by the Total Ozone Mapping Spectrometer (TOMS) satellite (Fig. 1b; Prospero et al., 2002). In summary, the core site likely receives terrestrial material from a mixture of local point sources, (which in turn receive material from the Namib and the plateau) as well as more distal sources from the Kalahari Desert and from the Etosha Pan. Thus, the main terrestrial catchment spans the area between about 17°S and 30°S and between the west coast and 25°E.

In addition to dust, a small amount of river-suspended material is transported from major rivers to the core site by ocean currents (Bremner and Willis, 1993). Two major rivers in this region are the Cunene River, which enters the ocean at about 17°S, and the Orange River at about 29°S, although most material from the Orange River is transported southwards (Bremner and Willis, 1993).

2.3 Leaf-wax δD as a recorder of δD_p

To understand past hydrological changes in southwestern Africa, we use δD of plant leaf wax *n*-alkanes. Leaf-wax δD is mainly controlled by the δD of precipitation (δD_p) and thus records the hydrological history of precipitation. However, in addition to δD_p, vegetation type and the relative humidity of near surface air are also thought to exert second-order controls on leaf-wax δD (e.g. Sachse et al., 2012). Studies have shown that C_4 grasses exhibit a greater apparent fractionation relative to meteoric water than C_3 trees (Sachse et al., 2012 and refs therein). Although, less information exists, CAM plants exhibit similar apparent fractionation factors to C_4 grasses (Sachse et al., 2012). Greater apparent fractionation factors for C_4 plants is thought to be caused by less

transpirational isotopic enrichment relative to C_3 trees and shrubs (Smith and Freeman, 2006). However, other studies suggest limited control of vegetation type on leaf-wax δD (Hou et al., 2008). In addition to transpiration, biosynthetic differences may exert some control on leaf-wax δD, and other plant physiological characteristics such as water use efficiency and leaf structure may also contribute to differences in apparent fractionation between plant types (Sachse et al. 2012). The seasonal timing of leaf-wax formation may also exert a bias on the hydrogen isotopic signal that is recorded (Sachse et al., 2012; Tipple et al., 2013). For southwestern Africa, where most vegetation growth is limited to the short wet season, there is probably a bias to the beginning of the wet season when most plant leaves are formed.

Evapotranspiration of water from soils and leaves is also controlled by the relative humidity of the atmosphere; lower relative humidity favors more evapotranspiration, leading to higher leaf-wax δD (Hou et al., 2008; Sachse et al., 2006). Although some studies (Kahmen et al., 2013b; Kahmen et al., 2013a) suggest that relative humidity is a major control on leaf-wax δD, others suggest that the control of relative humidity is minor (Feakins and Sessions, 2010; McInerney et al., 2011). If relative humidity exerts a large effect on our leaf-wax δD values, this would anyway act to amplify amount-effect changes: greater precipitation amount goes hand-in-hand with more humid conditions and both would cause lower leaf-wax δD.

2.4 Controls on modern leaf-wax $\delta^{13}C$ in southwestern Africa

To understand past vegetation changes in southwestern Africa, we analysed leaf wax $\delta^{13}C$. $\delta^{13}C$ in Africa has been interpreted as an indicator of C_3 versus C_4 vegetation (Castaneda et al., 2009; Schefuß et al., 2003; Tierney et al., 2010). Trees, herbs and shrubs normally use the C_3 pathway, while most grasses in Africa use the C_4 pathway (Castaneda et al., 2009, Vogts et al., 2009).

The vegetation in our core source-area (Namib Desert, Namibian Plateau, Kalahari) comprises mainly C_4 grasses and some C_3 trees, C_3 shrubs, C_3 herbs and CAM plants (White, 1983; Rommerskirchen et al., 2006; Leistner, 1967). C_3 trees are mostly restricted to areas where groundwater is accessible e.g. ephemeral river beds (Schachtschneider and February, 2010). C_3 grasses are sparse and make up only

179 5% of grass species in the southern Kalahari region (Ellis et al., 1980). CAM plants are abundant to
180 the south of our source area, in southern Namibia and South Africa (Carr et al., 2014) and they
181 exhibit a wide range of $\delta^{13}C$ values (Boom et al., 2013). However, given the distal location of this
182 region from our core site compared to the relatively proximal Namib, Namibian Plateau and the
183 Kalahari, it is unlikely that the leaf waxes in core MD08-3167 are dominated by contributions from
184 CAM plants.

185 Grasses are annual plants and are thus better suited to short wet season environments such as
186 southwestern Africa than perennial C_3 woody plants (Gritti et al., 2010; Clary, 2008). As such, a C_4
187 grass-dominated environment is indicative of a brief but relatively humid wet season i.e. high
188 seasonality (Clary, 2008). The interpretation of past shifts between C_3 and C_4 vegetation depends on
189 the climate setting. In relatively humid areas, past shifts towards C_4 (C_3) vegetation dominance are
190 normally interpreted to reflect a decrease (increase) in wet season length (Collins et al., 2011,
191 Schefuß et al., 2003). In arid areas, the interpretation has been made in the opposite sense with a
192 shift towards C_4 indicating more humid conditions (e.g. Chase et al., 2009), because greater water
193 availability permits an expansion of grasses into areas previously barren of vegetation. Given that
194 southwestern Africa is arid to semi-arid, the latter interpretation likely applies to our $\delta^{13}C$ values.

195 As well as shifts between C_4 and C_3 vegetation, $\delta^{13}C$ values of C_3 vegetation respond to changes in
196 aridity, due to the effect of stomatal conductance on ^{13}C discrimination (Farquhar et al., 1989;
197 Diefendorf et al., 2010; Tipple and Pagani, 2007), with higher $\delta^{13}C$ values expected under arid
198 conditions. In addition, C_3 plants, exhibit variation in $\delta^{13}C$ between different growth forms (Vogts et
199 al., 2009). However, because C_3 is not the dominant vegetation type in our region, there will be a
200 small contribution to the sedimentary $\delta^{13}C$ signal from the response of C_3 vegetation to aridity:
201 instead the signal is likely dominated by C_3-C_4 changes.

3 Methods

3.1 Sediment core age model

Stratigraphy for the upper part of core MD08-3167 (23.3152°S; 12.3768°E) is based on published radiocarbon ages of planktonic foraminifera (Collins et al., 2013a). For the lower part (below 515 cm), stratigraphy is based on correlation of XRF-scanner Ca/Fe ratio with that of core GeoB1711-4 (23.3150°S, 12.3766°E; **Fig. 2a**), located at the same coring site as MD08-3167. The age model for core GeoB1711-4 is based on radiocarbon ages of planktonic foraminifera for the upper part and correlation of benthic foraminiferal $\delta^{18}O$ (Little et al., 1997) with that of core MD95-2042 (37.7998°N; 10.1665°E; Shackleton et al., 2002; Shackleton et al., 2000) for the lower part (**Fig. 2b**). The age model of core MD95-2042 has been revised (Govin et al., 2013) and transferred onto the new AICC2012 ice core chronology (Bazin et al., 2013; Veres et al., 2013).

3.2 Major-element ratios

Major-element composition of cores MD08-3167 and GeoB1711-4 was determined with the Avaatech X-Ray Fluorescence core scanner at MARUM, University of Bremen. To assess the terrigenous versus marine-derived content of sediment core MD08-3167, XRF-scanner elemental intensities were converted to element concentrations using 89 dried and powdered samples, which were analysed with EDP-XRF spectroscopy (Collins et al., 2013b; Weltje and Tjallingii, 2008). Biogenic opal concentrations (**Supplementary Fig. 1**) were measured at MARUM following the protocol of Müller and Schneider (1993). We take the terrigenous component as the sum of the concentrations of the most abundant terrestrial-derived elements (Fe + Ti + K + Al + Si; after e.g. Schneider et al., 1997, Mulitza et al., 2008) and take the marine-derived biogenic component as the sum of Ca and biogenic opal concentrations. We estimate the terrigenous fraction as the relative proportion of the terrigenous component versus the marine component.

3.3 Lipid extraction and purification

Between 10ml and 20ml of sediment were sampled using 10ml plastic syringes, which yielded 6g to 9g of sediment (dry weight). Samples were oven dried at 40°C and homogenised. Squalane internal standard was added to the samples before extraction. Organic compounds were extracted with a DIONEX Accelerated Solvent Extractor (ASE 200) at 100°C and 1000 psi using a 9:1 mixture of dichloromethane to methanol for 5 minutes, which was repeated 3 times. Saturated hydrocarbon fractions were obtained using silica gel column chromatography (mesh size 60) with subsequent elution with hexane over $AgNO_3$-coated silica to remove unsaturated hydrocarbon compounds.

3.4 Sedimentary concentration of *n*-alkanes

The concentration of long-chain leaf wax *n*-alkanes in the saturated hydrocarbon fractions was assessed using a ThermoFischer Scientific Focus GC-FID. Concentrations for analysis were estimated by comparison with the external standard containing even numbered *n*-alkanes in the range C_{18}-C_{34} at a concentration 10 ng/µl that was run every 6 samples (n=14). Precision of the quantification based on the standard deviation of repeated standard measurements is 9%. The concentration of *n*-alkanes per gram sediment was estimated by comparison with the squalane internal standard. To remove the effect of changes in terrigenous- versus marine-derived material on the measured sedimentary *n*-alkane concentrations, *n*-alkane concentrations were normalised to the terrigenous fraction. Terrigenous-normalised concentrations therefore represent an estimate of the amount of *n*-alkane per gram of terrigenous sediment (ng. g terr sed^{-1}).

The origin of sedimentary *n*-alkanes was assessed with the Carbon Preference Index (CPI; Kolattukudy, 1976), the abundance ratio of odd- to even-numbered *n*-alkanes in the carbon number range C_{25} to C_{33}.

$$CPI_{25-33} = 0.5\left(\frac{C_{25}+C_{27}+C_{29}+C_{31}+C_{33}}{C_{24}+C_{26}+C_{28}+C_{30}+C_{32}}\right) + 0.5\left(\frac{C_{25}+C_{27}+C_{29}+C_{31}+C_{33}}{C_{26}+C_{28}+C_{30}+C_{32}+C_{34}}\right)$$

CPI is considered to be indicative of the contribution of *n*-alkanes from terrestrial plant leaf wax, (which have a strong odd over even preference; CPI > 1) versus those of petrogenic origin or other carbon pools subjected to diagenesis (CPI of ca. 1; Kolattukudy, 1976).

3.5 δD and $\delta^{13}C$ analysis of leaf-wax *n*-alkanes

δD values of *n*-alkanes were measured using a Thermo Trace GC coupled via a pyrolysis reactor operated at 1420°C to a Thermo Fisher MAT 253 isotope ratio mass spectrometer (GC/IR-MS). δD values were calibrated against external H_2 reference gas with δD of -235‰ VSMOW. The squalane internal standard (δD = -180‰) yielded an accuracy of 2‰ and a precision of 1‰ on average (n = 210). Repeated analysis (n = 43) of an external standard (a mixture of 12 *n*-alkanes between chain length C_{18} to C_{34}, δD ranging between -43‰ and -237‰) between every six analyses yielded a root-mean-squared accuracy of 2‰ and a standard deviation of on average 3‰. The H_3-factor had a mean of 6.37 ± 0.02 and varied between 6.35 and 6.42 throughout analyses. Samples were analysed in duplicate or triplicate. For the C_{31} *n*-alkane, the mean value of the standard deviation between replicates is 1‰.

Sedimentary δD values were corrected for the ice-volume effect. Past seawater δD enrichment was estimated based on the seawater $\delta^{18}O$ (Waelbroeck et al., 2002) and converted to δD using the global meteoric water line (Craig, 1961). These values were interpolated onto the age of each of the samples and subtracted from the measured leaf-wax δD values of the corresponding sample.

Compound-specific $\delta^{13}C$ analyses were carried out using a Thermo Trace GC Ultra coupled to a Finnigan MAT 252 isotope ratio monitoring mass spectrometer via a combustion interface operated at 1000°C. Isotope values were calibrated against external CO_2 reference gas with a $\delta^{13}C$ of -36.02‰ VPDB. Values are reported in the standard delta notation against the Vienna PeeDee Belemnite (VPDB) standard. All samples were run at least in duplicate, with a reproducibility of on average 0.1 ‰ for the C_{31} *n*-alkane. The squalane internal standard ($\delta^{13}C$ = -19.9‰) yielded an accuracy of 0.3‰ and a precision of 0.1‰ (n=151).

4. Results

Over the last 140 ka, the sedimentation rate of core MD08-3167 (**Fig. 3a**) displays low values during the last interglacial period (MIS 5.5; 5 cm.kyr^{-1}) and the Holocene (4 cm.kyr^{-1}), and an increase during the last glacial period (MIS 5.4 to MIS 2) with maximum values during the LGM (MIS 2; 27 cm.kyr^{-1}). The terrigenous fraction of the core (**Fig. 3b**) is lower during most of MIS 5, MIS 3 and MIS 1 and higher during MIS 2 and MIS 4.

CPI values for the sediment core have a mean of 5.4 ± 0.8 suggesting that the *n*-alkanes are mostly sourced from higher terrestrial plants and that the contribution from petrogenic or diagenetic sources is minor. Terrigenous-normalised concentrations of the sedimentary C_{31} *n*-alkane range between 600 µg. g terr sed^{-1} and 3500 µg.g terr sed^{-1} (**Fig. 3c**). Concentrations are highest during MIS 6, 3 and 2, and lowest during MIS 5 and 1. Concentrations also track precessional summer insolation variations (e.g. high values during the SH insolation maximum at 45 ka and low values during the minimum at 25 ka) although this is less pronounced during MIS 5 (**Fig. 3c**).

Sedimentary leaf-wax $\delta^{13}C$ values range between -24.4‰ ± 0.2‰ and -26.1‰ ± 0.4‰ for the C_{31} *n*-alkane, which is the most abundant homologue (**Fig. 2d**). The record displays higher values during the last glacial period relative to the Holocene and the last interglacial period (**Fig. 3e**). In addition to the glacial-interglacial variations, the $\delta^{13}C$ record also displays strong precessional-scale variations, with higher values during SH summer insolation maxima compared to minima.

Ice-volume corrected sedimentary leaf-wax δD values vary between -134‰ ± 1‰ and -156‰ ± 1‰ for the C_{31} *n*-alkane (**Fig. 3f**). Leaf-wax δD exhibits glacial-interglacial changes: δD values are lower during the last glacial period compared to the Holocene and the last interglacial period. Strong precessional-timescale variations are also evident: δD values are lower during SH summer insolation maxima relative to minima. Overall, lower δD values are coeval with higher leaf-wax $\delta^{13}C$ values and higher *n*-alkane concentrations.

5 Discussion

5.1 Terrigenous fraction and terrigenous-normalised *n*-alkane concentrations

The terrigenous fraction of the sediment is higher during MIS 2 and MIS 4 and lower during MIS 1, MIS 3 and most of MIS 5 (**Fig. 3b**). Changes in the terrigenous fraction depend on changes in either marine productivity or terrestrial input. Sedimentation rate (**Fig. 3a**) was lowest during the Holocene and last interglacial period, and higher during the last glacial period, particularly at MIS 2, suggesting that the increased terrigenous fraction during the glacial and particularly during MIS 2 was due to increased terrestrial sediment input. This may reflect increased tradewind strength during the last glacial period, as previously suggested (Shi et al., 2000). Additionally, because the Namib Desert is sediment-starved (Lancaster, 2000), increased terrestrial input probably indicates increased precipitation and flooding in the desert or in the upper catchment of the ephemeral rivers, which would have enhanced weathering and erosion, increasing the amount of fine material in the desert available for wind deflation (e.g. Rea, 1994). Other changes in terrigenous fraction not mirrored in the sedimentation rate are probably due to the dilution effect of marine productivity variations.

The terrigenous-normalised *n*-alkane concentrations were higher during SH summer insolation maxima and during the last glacial period versus the Holocene and the last interglacial period (**Fig. 3c**). This may indicate greater continental vegetation coverage during these periods. Alternatively, however, this may partly be reflecting the greater organic matter adsorption capacity of finer grain size sediments (Meyer, 1994) that were deposited off Namibia during the last glacial period (**Fig 3g**. Stuut et al., 2002).

5.2 Leaf-wax $\delta^{13}C$

5.2.1 Past vegetation changes in southwestern Africa

For the late Holocene section of the sediment core (last 4 ka) the *n*-C_{31} alkane exhibits a mean $\delta^{13}C$ value of -25.7‰ ± 0.4‰. We interpret this to represent a mixture of mainly C_4 grasses ($\delta^{13}C_{31}$ = -22.1‰; Rommerskirchen et al., 2006) with some contribution from C_3 trees ($\delta^{13}C_{31}$ = -34.0‰; Vogts

et al., 2009), C_3 shrubs ($\delta^{13}C_{31}$ = -34.4‰; Vogts et al., 2009), C_3 herbs ($\delta^{13}C_{31}$ = -35.7%; Vogts et al., 2009), and CAM plants ($\delta^{13}C_{31}$ = -25.9%; mean of FCAM and CAM; Boom et al., 2014).

Over the last 140ka, sedimentary leaf wax $\delta^{13}C$ values range between -24.4‰ and -26.1‰ (**Fig. 3d**), with variations on precessional and glacial-interglacial timescales. We suggest that $\delta^{13}C$ variations represent relative changes in the C_4 end-member versus the C_3 / CAM end-member. $\delta^{13}C$ values were higher (suggesting relatively more C_4 grasses) during SH summer insolation maxima and the last glacial period versus the Holocene and last interglacial period. We suggest these periods to represent increases in the absolute contribution from C_4 grasses, in line with evidence for increased grass charcoal abundance during SH summer insolation maxima in sediments off the coast of Namibia (Daniau et al., 2013).

The range of leaf-wax $\delta^{13}C$ values (-24.4‰ to -26.1‰), i.e. the amplitude of vegetation type changes, is small, indicating that C_4 grass vegetation has remained dominant relative to C_3 trees/shrubs or CAM plants in southwestern Africa over the past 140 ka. C_3 trees probably remained restricted to areas where groundwater was accessible.

5.2.2 Potential bias by CO_2 and source area shifts

Lower atmospheric CO_2 is thought to favour C_4 over C_3 photosynthesis (Collatz et al., 1998; Ehleringer et al., 1997) and thus could explain the relative increase in C_4 vegetation seen in our $\delta^{13}C$ record during the last glacial period relative to the Holocene and last interglacial period (**Fig. 3d**). However, CO_2 cannot explain the precessional timescale variability of leaf-wax $\delta^{13}C$, which is of larger magnitude than glacial-interglacial variability (**Fig. 3d**). This suggests that hydrology rather than CO_2 was the main control on C_3-C_4 shifts in southwestern Africa over the last 140 ka.

An alternative explanation for the downcore changes in leaf-wax $\delta^{13}C$ could be source-area shifts. For example, pollen data suggest that increased wind strength caused an increase in delivery of material from western South Africa during the last glacial period (Shi et al., 2000). However, in southern Namibia and South Africa modern vegetation displays lower leaf-wax $\delta^{13}C$ values due to the

dominance of C_3 and CAM vegetation (Boom, et al., 2014). Therefore, the glacial increase in C_4 cannot be explained by a southward shift of the source area.

5.2.3 Hydrological inferences from vegetation

Today the Namib and Kalahari Deserts are partly savanna vegetated, partly barren. Instrumental data indicate that during 2011, the wettest year on record (since 1962), most of the rain was delivered in a few rainy days and this transformed the barren gravel plains into savanna grassland (Eckardt et al., 2013). We suggest an analogous scenario to have taken place in southwestern Africa in the past: higher $\delta^{13}C$ (**Fig. 3d**) values during the last glacial period and insolation maxima indicate an expansion/thickening of C_4 grasses across barren areas of the Namib Desert, Namibian Plateau and Kalahari Desert due to increased SH summer rainfall. These periods hence represent maxima in seasonality, in line with Daniau et al., (2013). The dominance of C_4 grasses over C_3 vegetation throughout the record suggests that semi-arid conditions and high seasonality were a persistent feature of southwestern African climate over the past 140ka. This is in line with indications of the persistence of aridity based on sedimentary landforms in this region (Lancaster, 2002; Stone and Thomas, 2012).

5.3 Past leaf-wax δD

Although leaf-wax δD is commonly interpreted to reflect past δD_p, the extent to which vegetation-type changes may have controlled leaf-wax δD first needs to be assessed. The magnitude of the downcore C_3-C_4 vegetation-type changes is small (maximum $\delta^{13}C$ change 1.7‰). Based on existing fractionation factors for C_3 (-123‰; Sachse et al., 2012) and C_4 (-139‰) vegetation, the maximum leaf-wax δD shift caused by vegetation changes would be about 2‰. This would hence argue against vegetation-type changes as the main cause of the past leaf-wax δD variations. Nonetheless, more work is needed to assess fractionation factors for vegetation types specific to southwestern Africa.

Given that δD changes associated with vegetation type appear to be small, we interpret past leaf-wax δD to represent changes in δD_p and relative humidity. As described above (section 2.3), environmental controls on δD_p are complex: past δD_p in southwestern Africa may have been

controlled by local precipitation amount, non-local precipitation amount and/or changes in the dominant moisture source. Lower δD_p values would imply greater local amount, greater non-local amount and/or greater proportion of Indian-sourced moisture. Given that precessional and glacial-interglacial timescale shifts towards C_4 vegetation (wetter conditions; **Fig. 3d**) were coeval with periods of lower leaf-wax δD (**Fig. 3f**), it is likely that lower (higher) δD_p values at least partly reflect an increase (decrease) in local precipitation amount. We cannot completely rule out that non-local precipitation changes (for example increased rainout over southeastern Africa), or moisture source changes (increased amount of Indian Ocean-sourced moisture) are partly responsible for periods of lower past δD_p. For example, a shift to more Indian Ocean moisture during the last glacial period (Collins et al., 2013a) may explain the larger glacial-interglacial leaf-wax δD difference (**Fig. 3f**) compared to the glacial-interglacial $\delta^{13}C$ difference (**Fig. 3d**). Reduced Atlantic Ocean moisture may have been associated with a colder and northward shifted Benguela Current during the last glacial period (Jansen et al., 1996, Ufkes et al., 2000). Overall, we take lower leaf-wax δD to represent an increase in local amount with some overprint from increased non-local precipitation and increased proportion of Indian Ocean-sourced moisture. In addition, relative humidity changes would have shifted leaf-wax δD in the same direction (more humid conditions, lower leaf wax δD) thus enhancing the hydrologic signal.

Given that the isotopic signature recorded by leaf wax *n*-alkanes was likely 'locked in' early in the growth season (Tipple et al., 2013) and also considering that the amount-effect operates on sub-seasonal timescales (Risi et al., 2008b), our leaf-wax δD data point to more intense early SH summer precipitation during SH summer insolation maxima and during the last glacial period versus the Holocene and last interglacial period.

5.4 Comparison with other climate records

On precessional timescales, increased summer precipitation in southwestern Africa during SH summer insolation maxima (**Fig. 3d, f**) is in agreement with the record from Lake Tswaing in South Africa (Partridge et al., 1997; see location in Fig. 1b), and with relatively dry conditions during the

mid-Holocene insolation minimum within the Zambezi River catchment in southeastern Africa (Schefuß et al., 2011). Together these records and ours would suggest that SH summer insolation maxima resulted in wetter conditions throughout most of southern Africa. However, our record contrasts with the hyrax-midden record from the Namib Desert (Chase et al., 2009; Fig. 1b), which indicates wetter conditions during the mid-Holocene SH summer insolation minimum. Although the Holocene is less well-resolved in our record, it is clear for the rest of our record that SH summer insolation minima were drier. One possible explanation for the mismatch may relate to the source areas of the two records. The hyrax-midden record reflects the climate of the hyraxes' habitat (in close proximity to the midden), situated in the Namib Desert. Our record reflects a wider catchment including material from the Namibian plateau (Eckardt and Kuring, 2005) and the Kalahari Desert (Prospero et al., 2002), further east of the Namib. Consequently, climate in the Namibian Desert may indeed respond in phase with NH summer insolation, perhaps via a control by upwelling intensity, while the Namibian plateau and the Kalahari Desert respond in phase with SH summer insolation. Further records or model simulations are needed to verify this hypothesis.

On glacial-interglacial timescales, our data suggest increased summer precipitation during the last glacial period relative to the Holocene and last interglacial period. This is consistent with the deposition of river-derived silts (the 'Homeb silts') in the Namib Desert during the LGM, thought to indicate increased flow of ephemeral rivers due to wetter conditions on the Namibian plateau (Heine and Heine, 2002). Our record is also in agreement with the grain-size record (Stuut et al., 2002) from the Walvis Ridge (**Fig. 1a**) which indicates the deposition of finer material during the last glacial period (**Fig. 3g**), thought to reflect increased river derived material southwestern Africa and perhaps also attributable to increased flow of ephemeral rivers. Enhanced tropical precipitation in southern Africa during the last glacial period is also in agreement with climate models (e.g. Kageyama et al., 2013) and this would explain lower leaf-wax δD in other southwestern African cores during the LGM relative to the Holocene (Collins et al 2013a).

In order to understand the interplay between the climate of southwestern African and tropical Central Africa, we also compare our record with a record of major-element composition (Schneider et al., 1997) from a site at 6°S (**Fig. 1a**) which reflects Congo River discharge and hence wetness in central Africa. The Congo River record **(Fig. 3h)** indicates wetter conditions during NH summer maxima (i.e. during SH summer insolation minima), and also during the Holocene and last interglacial period, relative to the last glacial period. This response is hence in antiphase to our leaf-wax δD record from further south (23°S; **Fig. 3f)**. This implies that SH summer insolation maxima and glacial boundary conditions acted to cause an (albeit minor) enhancement of precipitation in southwestern Africa coeval with drier conditions in central Africa.

5.5 Possible climate mechanisms

In terms of the effect of precessional insolation variability, more humid periods during insolation maxima likely represent enhanced northerly East African monsoon, which would have brought more moisture into southern Africa, enhancing precipitation. This mechanism would also explain the precessional-timescale antiphase between central Africa and southwestern Africa: in central Africa NH insolation is thought to control the on-land moisture flux (Schneider et al., 1997).

The effect of glacial boundary conditions is more complicated. One explanation for wetter conditions is that winter westerlies shifted north during the last glacial period (Chase and Meadows, 2007; Cockcroft et al., 1987; Stuut et al., 2002). However, lower leaf-wax δD values (**Fig. 3f**) argue against a shift towards more proximal Atlantic Ocean-sourced westerly precipitation. Moreover, westerly-influenced C_3 vegetation (Boom et al., 2014, Carr et al., 2014) did not shift northward during the last glacial period (**Fig. 3d**). Finally, the strong precessional signal throughout our record (**Fig. 3d,f**) suggests a continuous influence of the summer monsoon and both were at a maximum in southwestern Africa at the LGM: a simultaneous influence from mid-latitude winter westerly precipitation at the LGM would have required extreme seasonal shifts in the climate belts. Overall, it is unlikely that a wetter glacial was due to increased precipitation from the winter westerlies. We

449 suggest that the increased glacial wetness was due to more tropical summer precipitation, mainly
450 from TTTs.

451 Although wetter conditions during the last glacial period in southwestern Africa (**Fig. 3d, f**) were
452 coeval with drier conditions in the Congo Basin (**Fig. 3h**), this is unlikely to be due to a
453 straightforward displacement of the tropical precipitation from the Congo Basin towards
454 southwestern Africa because the southern boundary of the rainforest belt was shifted equatorward
455 in western Africa during the LGM (Collins et al., 2011; Dupont et al., 2008; Ning and Dupont, 1997; in
456 turn suggesting a wider SH savanna belt during the last glacial period). Instead, the glacial-interglacial
457 antiphase may represent an increase of the northerly East African monsoon (Indian Ocean) at the
458 expense of the Central African monsoon (Atlantic Ocean) similar to the mechanism on precessional
459 timescales. This was perhaps associated with the relatively cold glacial SE Atlantic Ocean (Jansen et
460 al., 1996; Kim et al., 2003) compared with the relatively warm glacial Indian Ocean (Sonzogni et al.,
461 1998).

462 ## 6 Conclusions

463 We have used a sedimentary record of leaf-wax δD and $\delta^{13}C$ to reconstruct the hydroclimate of
464 southwestern Africa over the past 140 ka. Leaf-wax δD and $\delta^{13}C$ indicate increased summer
465 precipitation greater seasonality during SH summer insolation maxima relative to minima. Similarly,
466 SH summer precipitation was increased during the last glacial period versus the Holocene and last
467 interglacial period, with wettest conditions during the LGM. *n*-Alkane concentrations normalised to
468 the terrestrial sediment fraction support this interpretation. The dominance of C_4 vegetation
469 throughout the record indicates that southwestern Africa remained semi-arid over the last 140 ka.
470 More negative leaf-wax δD, the strong precessional signal and dominance of C_4 vegetation point to
471 the tropical monsoon as the dominant source of increased rainfall during the last glacial period
472 rather than the winter-westerlies. The hydroclimate of southwestern African responded in antiphase
473 with that of central Africa. This seems to reflect a competing behavior of the Atlantic Ocean- versus
474 Indian Ocean-sourced monsoonal systems over the last 140 ka.

Acknowledgements

We are grateful to Britta Beckmann and Ralph Kreutz for assistance in the lab and to Marco Klann for performing the opal measurements. We gratefully acknowledge the RETRO consortium for providing samples. The project was supported by the Helmholtz Climate Initiative REKLIM (Regional Climate Change) and the DFG Research Centre/Cluster of Excellence 'The Ocean in the Earth System'. The data presented here are available on the Pangaea database (www.pangaea.de).

References

Bazin, L., et al., 2013. An optimized multi-proxy, multi-site Antarctic ice and gas orbital chronology (AICC2012): 120-800 ka. Clim. Past 9, 1715-1731.

Boom, A., Carr, A. S., Chase, B. M., Grimes, H. L., & Meadows, M. E., 2014. Leaf wax *n*-alkanes and $\delta^{13}C$ values of CAM plants from arid southwest Africa. Org. Geochem. 67, 99-102.

Bremner, J.M., Willis, J.P., 1993. Mineralogy and geochemistry of the clay fraction of sediments from the Namibian continental margin and the adjacent hinterland. Marine Geology 115, 85-116.

Carr, A. S., et al. 2014. Leaf wax *n*-alkane distributions in arid zone South African flora: Environmental controls, chemotaxonomy and palaeoecological implications. Org. Geochem. 67, 72-84.

Castañeda, I.S., et al., 2009. Wet phases in the Sahara/Sahel region and human migration patterns in North Africa. Proc. Natl. Acad. Sci. U.S.A. 106, 20159-20163.

Chase, B.M., Meadows, M.E., 2007. Late Quaternary dynamics of southern Africa's winter rainfall zone. Earth Sci. Rev. 84, 103-138.

Chase, B.M., et al., 2009. A record of rapid Holocene climate change preserved in hyrax middens from southwestern Africa. Geology 37, 703-706.

Clary, J., 2008. Rainfall seasonality determines annual/perennial grass balance in vegetation of Mediterranean Iberian. Plant Ecology 195, 13-20.

Cockcroft, M.J., et al., 1987. The application of a present-day climatic model to the late quaternary in southern Africa. Clim. Change 10, 161-181.

Collatz, G.J., et al., 1998. Effects of climate and atmospheric CO_2 partial pressure on the global distribution of C_4 grasses: present, past, and future. Oecologia 114, 441-454.

Collins, J. A., et al., 2013a. Estimating the hydrogen isotopic composition of past precipitation using leaf-waxes from western Africa. Quat. Sci. Revs. 65, 88-101.

Collins, J., et al., 2013b. Abrupt shifts of the Sahara–Sahel boundary during Heinrich stadials. Clim. Past 9, 1181-1191.

Collins, J.A., et al., 2011. Interhemispheric symmetry of the tropical African rainbelt over the past 23,000 years. Nat. Geosci. 4, 42-45.

Craig, H., 1961. Isotopic variations in meteoric waters. Science 133, 1702-1703

Daniau, A.-L., et al., 2013. Orbital-scale climate forcing of grassland burning in southern Africa. Proc. Natl. Acad. Sci., 110, 5069-5073.

Dansgaard, W., 1964. Stable isotopes in precipitation. Tellus 16, 436-468.

Diefendorf, A.F., et al., 2010. Global patterns in leaf ^{13}C discrimination and implications for studies of past and future climate. Proc. Natl. Acad. Sci., 107, 5738-5743.

Dupont, L.M., et al., 2008. Thirty thousand years of vegetation development and climate change in Angola (Ocean Drilling Program Site 1078). Clim. Past 4, 107-124.

Eckardt, F.D., Kuring, N., 2005. SeaWiFS identifies dust sources in the Namib Desert. Intl J. Rem. Sens 26, 4159-4167.

Eckardt, F.D., et al., 2013. The nature of moisture at Gobabeb, in the central Namib Desert. J. Arid Env. 93, 7-19.

Eglinton, G., Hamilton, R.J., 1967. Leaf epicuticular waxes. Science 156, 1322-1335.

Ehleringer, J.R., et al., 1997. C4 photosynthesis, atmospheric CO2, and climate. Oecologia 112, 285-299.

Ellis, R., Vogel, J. C., & Fuls, A., 1980. Photosynthetic pathways and the geographical distribution of grasses in South West Africa/Namibia. South African Journal of Science, 76, 307-314.

Farquhar, G. D., Hubick, K, T., Condon, A. G., Richards, R. A., 1989. Carbon isotope fractionation and plant water-use efficiency. Stable Isotopes in Ecological Research. Ecological Studies 68, 21-40

533 Feakins, S.J., Sessions, A.L., 2010. Controls on the D/H ratios of plant leaf waxes in an arid
534 ecosystem. Geochim. Cosmochim. Acta 74, 2128-2141.

535 Gimeno, L., et al., 2010. On the origin of continental precipitation. Geophys. Res. Lett. 37,
536 L13804.

537 Govin, A., 2013. Terrigenous input off northern South America driven by changes in
538 Amazonian climate and the North Brazil Current retroflection during the last 250 ka, Clim. Past
539 Disc., 9, 5855-5898, 10.5194/cpd-9-5855-2013.

540 Gritti, E.S., et al., 2010. Simulated effects of a seasonal precipitation change on the
541 vegetation in tropical Africa. Clim. Past 6, 169-178.

542 Harrison, M., 1984. A generalized classification of South African summer rain-bearing
543 synoptic systems. Int. J. Climatol. 4, 547-560.

544 Heine, K., Heine, J.T., 2002. A paleohydrologic reinterpretation of the Homeb Silts, Kuiseb
545 River, central Namib Desert (Namibia) and paleoclimatic implications. Catena 48, 107-130.

546 Hou, J., et al., 2008. Can sedimentary leaf waxes record D/H ratios of continental
547 precipitation? Field, model, and experimental assessments. Geochim. Cosmochim. Acta 72, 3503-
548 3517.

549 IAEA/WMO, 2006. Global Network of Isotopes in Precipitation. The GNIP Database.
550 Accessible at: http://www.iaea.org/water.

551 Jansen, J. H. F., Ufkes, E., & Schneider, R. R., 1996. Late Quaternary movements of the
552 Angola-Benguela Front, SE Atlantic, and implications for advection in the equatorial ocean. In The
553 South Atlantic (pp. 553-575). Springer Berlin Heidelberg.

554 Kageyama, M., et al., 2013. Mid-Holocene and Last Glacial Maximum climate simulations
555 with the IPSL model—part I: comparing IPSL_CM5A to IPSL_CM4. Clim. Dyn. 40, 2447-2468.

556 Kahmen, A., et al., 2013b. Leaf water deuterium enrichment shapes leaf wax n-alkane δD
557 values of angiosperm plants II: Observational evidence and global implications. Geochim.
558 Cosmochim. Acta 111, 50-63.

559 Kahmen, A., et al., 2013a. Leaf water deuterium enrichment shapes leaf wax *n*-alkane dD
560 values of angiosperm plants I: Experimental evidence and mechanistic insights. Geochim.
561 Cosmochim. Acta 111, 39-49.

562 Kim, J. H., Schneider, R. R., Mulitza, S., & Müller, P. J., 2003. Reconstruction of SE trade-
563 wind intensity based on sea-surface temperature gradients in the Southeast Atlantic over the last
564 25 kyr. Geophys. Res. Lett 30, 2144, doi: 10.1029/2003GL017557, 22.

565 Koch, K., Ensikat, H.-J., 2008. The hydrophobic coatings of plant surfaces: epicuticular wax
566 crystals and their morphologies, crystallinity and molecular selfassembly. Micron 39, 759-772.

567 Kolattukudy, P.E., 1976. Chemistry and Biochemistry of Natural Waxes. Elsevier Scientific
568 Pub. Co., Amsterdam, New York.

569 Kukla, G.J., et al., 2002. Last interglacial climates. Quaternary Res. 58, 2-13.

570 Lancaster, N., 2002. How dry was dry?-Late Pleistocene palaeoclimates in the Namib
571 Desert. Quat. Sci. Rev. 21, 769-782.

572 Leistner, O. A., 1967. The plant ecology of the southern Kalahari. *Bot. Survey Mem. 38*
573 *Pretoria: Dep. Agric. Tech. Serv., Bot. Res. Inst.*

574 Leroux, M., 1983. The Climate of Tropical Africa, Atlas, 3-9, Champion, Paris, pp. 39-45.

575 Lisiecki, L.E., Raymo, M.E., 2005. A Pliocene-Pleistocene stack of 57 globally distributed
576 benthic $\delta^{18}O$ records. Paleoceanography 20.

577 McInerney, F.A., et al., 2011. Hydrogen isotope ratios of leaf wax n-alkanes in grasses are
578 insensitive to transpiration. Geochim. Cosmochim. Acta 75, 541-554.

579 Meyer, L. M.,1994. Relationships between mineral surfaces and organic carbon
580 concentrations in soils and sediments. Chemical Geology, 114, 347-363.

581 Müller, P.J., Schneider, R., 1993. An automated leaching method for the determination of
582 opal in sediments and particulate matter. Deep Sea Res. Part I 40, 425-444.

583 Mulitza, S., et al., 2008. Sahel megadroughts triggered by glacial slowdowns of Atlantic
584 meridional overturning. Paleoceanography 23, DOI: 10.1029/2008PA001637

585 Ning, S., Dupont, L., 1997. Vegetation and climatic history of southwest Africa: A marine
586 palynological record of the last 300,000 years. Veget. Hist. Archaebot. 6, 117-131.

587 Olivier, J., 1995. Spatial distribution of fog in the Namib. J. Arid Env. 29, 129-138.

588 Partridge, T.C., et al., 1997. Orbital forcing of climate over South Africa: A 200,000-year
589 rainfall record from the pretoria saltpan. Quat. Sci. Rev. 16, 1125-1133.

590 Pausata, F.S.R., et al., 2011. Chinese stalagmite $\delta^{18}O$ controlled by changes in the Indian

591 monsoon during a simulated Heinrich event. Nat. Geosci. 4, 474-480.

592 Pokras, E.M., Mix, A.C., 1985. Eolian evidence for spatial variability of late Quaternary
593 climates in tropical Africa. Quaternary Res. 24, 137-149.

594 Prospero, J.M., et al., 2002. Environmental characterization of global sources of atmospheric
595 soil dust identified with the Nimbus 7 Total Ozone Mapping Spectrometer (TOMS) absorbing
596 aerosol product. Rev. Geophys. 40, 31.

597 Rea, D.K., 1994. The paleoclimatic record provided by eolian deposition in the deep sea:
598 The geologic history of the wind. . Rev. Geophys. 32, 159-195.

599 Risi, C., et al., 2008a. Influence of convective processes on the isotopic composition ($\delta^{18}O$
600 and δD) of precipitation and water vapor in the tropics: 2. Physical interpretation of the amount
601 effect. J. Geophys. Res. 113, D19306.

602 Risi, C., et al., 2008b. What controls the isotopic composition of the African monsoon
603 precipitation? Insights from event-based precipitation collected during the 2006 AMMA field
604 campaign. Geophys. Res. Lett. 35, L24808.

605 Rommerskirchen, F., Plader, A., Eglinton, G., Chikaraishi, Y., & Rullkötter, J., 2006.
606 Chemotaxonomic significance of distribution and stable carbon isotopic composition of long-chain
607 alkanes and alkan-1-ols in C4 grass waxes. Organic Geochemistry, 37, 1303-1332.

608 Rossignol-Strick, M., 1985. Mediterranean Quaternary sapropels, an immediate response of
609 the African monsoon to variation of insolation. Palaeogeogr. Palaeoclimatol. Palaeoecol. 49, 237-
610 263.

611 Rouault, M., Florenchie, P., Fauchereau, N., & Reason, C. J., 2003. South East tropical
612 Atlantic warm events and southern African rainfall. Geophysical Research Letters, 30(5).

613 Sachse, D., et al., 2012. Molecular Paleohydrology: Interpreting the Hydrogen-Isotopic
614 Composition of Lipid Biomarkers from Photosynthesizing Organisms. Ann. Rev. Earth Plan. Sci.
615 40, 221-249.

616 Sachse, D., et al., 2004. Hydrogen isotope ratios of recent lacustrine sedimentary *n*-alkanes
617 record modern climate variability. Geochim. Cosmochim. Acta 68, 4877-4889.

618 Sachse, D., et al., 2006. dD values of individual *n*-alkanes from terrestrial plants along a
619 climatic gradient - Implications for the sedimentary biomarker record. Org. Geochem. 37, 469-483.

620 Schefuß, E., et al., 2011. Forcing of wet phases in southeast Africa over the past 17,000
621 years. Nature 480, 509-512.

622 Schachtschneider K. and February E. C., 2010. The relationship between fog, floods,
623 groundwater and tree growth along the Lower Kuiseb River in the hyperarid Namib. J. Arid Env 74,
624 1632-1637.

625 Schefuß, E., et al., 2003. African vegetation controlled by tropical sea surface temperatures
626 in the mid-Pleistocene period. Nature 422, 418-421.

627 Schefuß, E., et al., 2005. Climatic controls on central African hydrology during the past
628 20,000 years. Nature 437, 1003-1006.

629 Schneider, R.R., et al., 1997. Monsoon Related Variations in Zaire (Congo) Sediment Load
630 and Influence of Fluvial Silicate Supply on Marine Productivity in the East Equatorial Atlantic During
631 the Last 200,000 Years. Paleoceanography 12.

632 Servain, J., & Legler, D. M. 1986. Empirical orthogonal function analyses of tropical Atlantic
633 sea surface temperature and wind stress: 1964–1979. Journal of Geophysical Research: Oceans
634 (1978–2012), 91(C12), 14181-14191.

635 Shackleton, N.J., et al., 2002. The classic Marine Isotope Substage 5e. Quaternary Res. 58,
636 14-16.

637 Shackleton, N.J., et al., 2000. Phase Relationships Between Millennial-Scale Events 64,000-
638 24,000 Years Ago. Paleoceanography 15, 565-569.

639 Shi, N., et al., 2000. Correlation between Vegetation in Southwestern Africa and Oceanic
640 Upwelling in the Past 21,000 Years. Quaternary Res. 54, 72-80.

641 Shi, N., et al., 2001. Southeast trade wind variations during the last 135 kyr: evidence from
642 pollen spectra in eastern South Atlantic sediments. Earth Planet. Sci. Lett. 187, 311-321.

643 Smith, F.A., Freeman, K.H., 2006. Influence of physiology and climate on δD of leaf wax *n*-
644 alkanes from C_3 and C_4 grasses. Geochim. Cosmochim. Acta 70, 1172-1187.

645 Sonzogni, C., Bard, E., & Rostek, F., 1998. Tropical sea-surface temperatures during the last
646 glacial period: a view based on alkenones in Indian Ocean sediments. Quat. Sci. Rev. 17, 1185-
647 1201.

648 Still, C.J., Powell, R.L., 2010. Continental-scale distributions of plant stable carbon isotopes,
649 in: West, J.B., Bowen, G.J., Dawson, T.E., and K. Tu (Ed.), Isoscapes: Understanding movement,
650 pattern, and process on Earth through isotope mapping. Springer, Dordrecht.

651 Stone, A.E.C., Thomas, D.S.G., 2012. Casting new light on late Quaternary environmental
652 and palaeohydrological change in the Namib Desert: A review of the application of optically
653 stimulated luminescence in the region. J. Arid Env 93, 40-58.

Stuut, J.-B.W., et al., 2002. A 300-kyr record of aridity and wind strength in southwestern Africa: inferences from grain-size distributions of sediments on Walvis Ridge, SE Atlantic. Marine Geology 180, 221-233.

Tierney, J.E., et al., 2010. A molecular perspective on Late Quaternary climate and vegetation change in the Lake Tanganyika basin, East Africa. Quat. Sci. Rev. 29, 787-800.

Tierney, J. E., Russell, J. M., Sinninghe Damsté, J. S., Huang, Y., & Verschuren, D., 2011. Late Quaternary behavior of the East African monsoon and the importance of the Congo Air Boundary. Quat. Sci. Rev, 30, 798-807.

Tipple, B.J., et al., 2013. Leaf-wax n-alkanes record the plant–water environment at leaf flush. Proc. Natl. Acad. Sci. U.S.A 110, 2659-2664.

Tipple, B.J., Pagani, M., 2007. The early origins of terrestrial C4 photosynthesis. Annu. Rev. Earth Planet. Sci. 35, 435-461.

Todd, M.C., et al., 2004. Water vapour transport associated with tropical–temperate trough systems over southern Africa and the southwest Indian Ocean. Int. J. Clim. 24, 555-568.

Tyson, P.D., 1986. Climatic change and variability in Southern Africa. Oxford University Press.

Ufkes, E., Jansen, J. H. F., & Schneider, R. R., 2000. Anomalous occurrences of Neogloboquadrina pachyderma (left) in a 420-ky upwelling record from Walvis Ridge (SE Atlantic). Marine Micropaleontology, 40(1), 23-42.

Urrego, D.H., et al., 2013. Increased aridity in southwestern Africa during the last-interglacial warmest periods. Clim. Past Disc. 9, 4323-4363.

Veres, D., et al., 2013. The Antarctic ice core chronology (AICC2012): an optimized multi-parameter and multi-site dating approach for the last 120 thousand years. Clim. Past 9, 1733-1748.

Vogts, A., Moossen, H., Rommerskirchen, F., & Rullkötter, J., 2009. Distribution patterns and stable carbon isotopic composition of alkanes and alkan-1-ols from plant waxes of African rain forest and savanna C_3 species. Org. geochem., 40, 1037-1054

Waelbroeck, C., et al., 2008. Scientific report of the MD167/ RETRO II IMAGES XVI cruise. Les rapports de campagnes a la mer. Institut Polaire Francais Paul Emile Victor, Plouzane, France, p. 137 pp.

Waelbroeck, C., et al., 2002. Sea-level and deep water temperature changes derived from benthic foraminifera isotopic records. Quat. Sci. Rev. 21, 295-305.

Weltje, G.J., Tjallingii, R., 2008. Calibration of XRF core scanners for quantitative geochemical logging of sediment cores: Theory and application. Earth Planet. Sci. Lett. 274, 423-438.

White, F., 1983. The vegetation of Africa: A descriptive memoir to accompany the UNESCO/AETFAT/UNSO vegetation map of Africa (Natural Resources Research 20). UN Educational, Scientific and Cultural Organization, Paris.

Figure Captions

Figure 1. a) Map of central and southern Africa showing precipitation distribution during SH summer (February). Congo Air Boundary (CAB) and Intertropical Convergence Zone (ITCZ) are marked. Benguela Current, Angola Current and Angola Benguela Front (ABF) are shown. Red diamond marks site of core MD08-3167 (this study). **b)** Precipitation distribution during SH winter (August). Dust sources, which are mostly active in SH winter, are shown: thin arrows highlight ephemeral rivers and pans in the vicinity of the core site that act as sources of dust (Eckardt and Kuring, 2005). Isolines on map mark dust sources identified with TOMS (Prospero et al., 2002): M and E mark Makgadikgadi Basin and Etosha Pan dust sources, respectively, and units are number of days per month when absorbing aerosol index exceeds 0.7. Study sites referred to in the text are given as white dots: Lake Tswaing (Partridge et al., 1997); Spitzkoppe hyrax midden (Chase et al., 2009); GeoB1008-3, Congo River (Schneider et al., 1997) and MD96-2094, Walvis Ridge (Stuut et al., 2002).

Figure 2. Derivation of age model for MD08-3167. a) Blue line is ln(Ca/Fe) ratio of GeoB1711-4. Green line is ln(Ca/Fe) of MD08-3167. Age model of MD08-3167 is based on ^{14}C ages (triangles) and correlation of Ca/Fe with GeoB1711-4 (Little et al., 1997; tie-points are marked as diamonds). b) Black line is benthic $\delta^{18}O$ of MD95-2042 (Shackleton et al., 2000; 2002). The age model of MD95-2042 has been revised (Govin et al., 2013) based on the AICC timescale (Bazin et al., 2013; Veres et al., 2013). Blue line is benthic $\delta^{18}O$ of GeoB1711-4 (Little et al., 1997). Age model of GeoB1711-4 is based ^{14}C dating (triangles) and correlation of benthic $\delta^{18}O$ with MD95-2042 (tie-points are marked as diamonds).

Figure 3. Sedimentary climate indicators of southwestern Africa from core MD08-3167 compared with other African climate records over the last 140 ka. **a)** Sedimentation rate of MD08-3167 based on age model. **b)** Terrigenous fraction of sediment core MD08-3167. **c)** Terrigenous-normalised sedimentary *n*-alkane concentration of MD08-3167 (light brown line) and February insolation at 25°S (red dashed line). **d)** $\delta^{13}C$ of the *n*-C_{31} alkane of MD08-3167 (green line; error bars represent 1sigma reproducibility of replicates) and February insolation at 25°S (red dashed line). **e)** LR04 benthic $\delta^{18}O$ stack (Lisiecki and Raymo, 2005), reflecting global ice volume (blue dashed line). **f)** δD of the *n*-C_{31} alkane from MD08-3167 corrected for ice volume (black line) and February insolation at 25°S (red dashed line). **g)** Grain-size aridity index from core MD96-2094; 20°S; Walvis Ridge (Stuut et al., 2002). **h)** Al/K from core GeoB1008-3 at 6°S, an indicator of Congo River discharge (Brown line; Schneider et al., 1997) and August insolation at 20°N (red dashed line). Marine Isotope Stages (MIS) are indicated above the age scale.

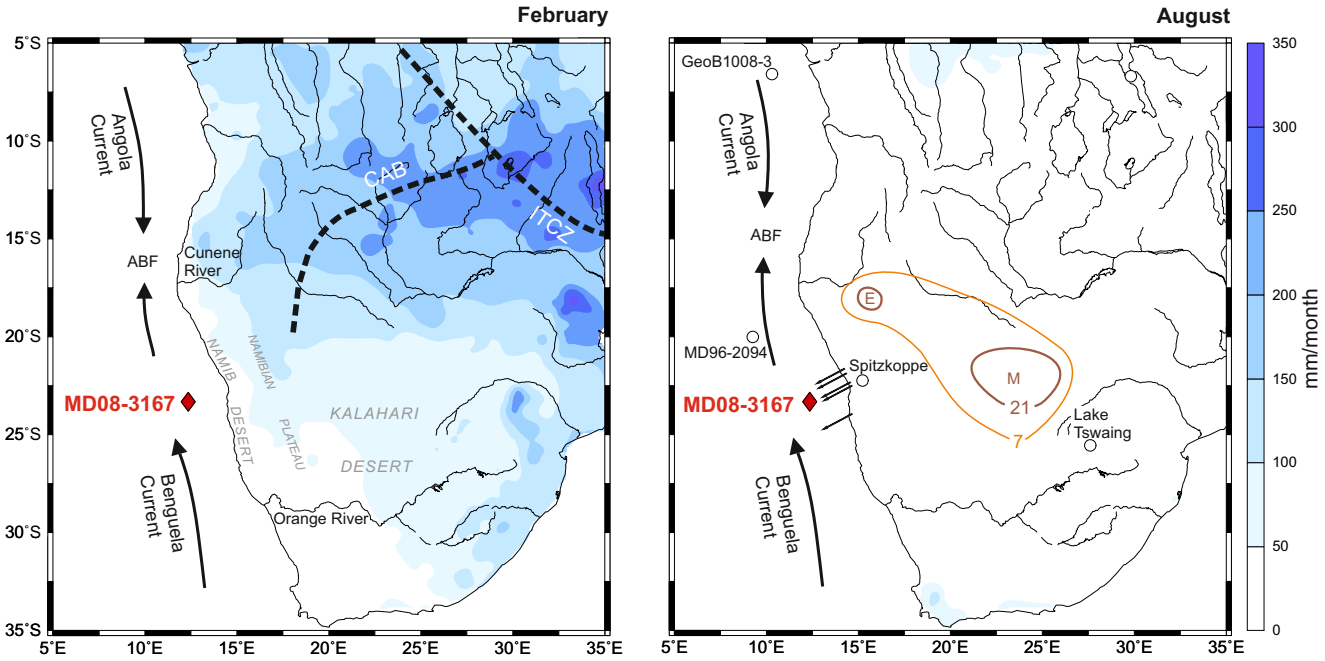
February
August
5°S
10°S
15°S
20°S
25°S
30°S
35°S
5°E
10°E
15°E
20°E
25°E
30°E
35°E
Angola Current
ABF
Cunene River
CAB
ITCZ
NAMIB
DESERT
NAMIBIAN
PLATEAU
KALAHARI
DESERT
MD08-3167
Benguela Current
Orange River
GeoB1008-3
MD96-2094
Spitzkoppe
E
M
21
7
Lake Tswaing
350
300
250
200
150
100
50
0
mm/month

Figure 1

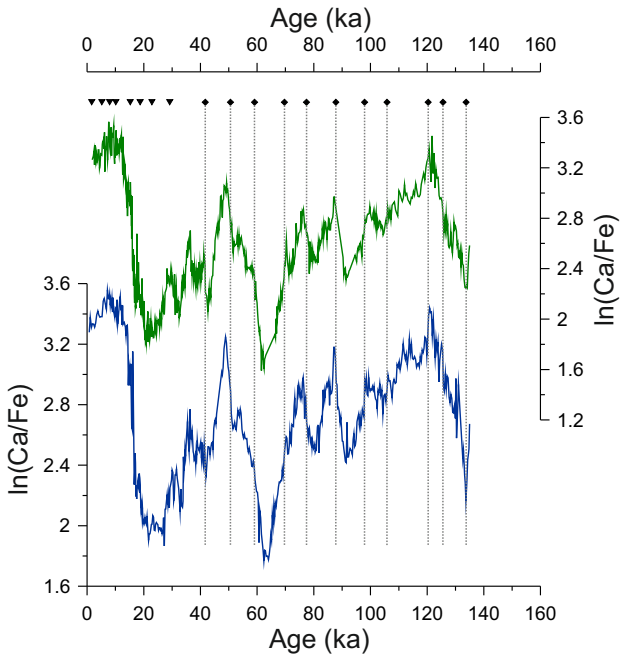
Age (ka)
0 20 40 60 80 100 120 140 160
ln(Ca/Fe)
3.6 3.2 2.8 2.4 2 1.6
1.6 2 2.4 2.8 3.2 3.6
Age (ka)
0 20 40 60 80 100 120 140 160
ln(Ca/Fe)
1.2 1.6 2 2.4 2.8 3.2 3.6

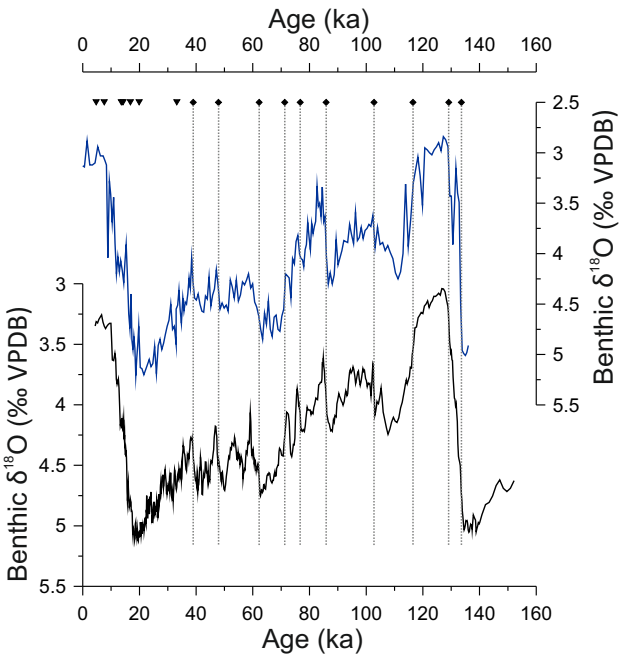
Age (ka)
0 20 40 60 80 100 120 140 160
Benthic δ18O (‰ VPDB)
3 3.5 4 4.5 5 5.5
Benthic δ18O (‰ VPDB)
2.5 3 3.5 4 4.5 5 5.5
Age (ka)
0 20 40 60 80 100 120 140 160

Figure 2

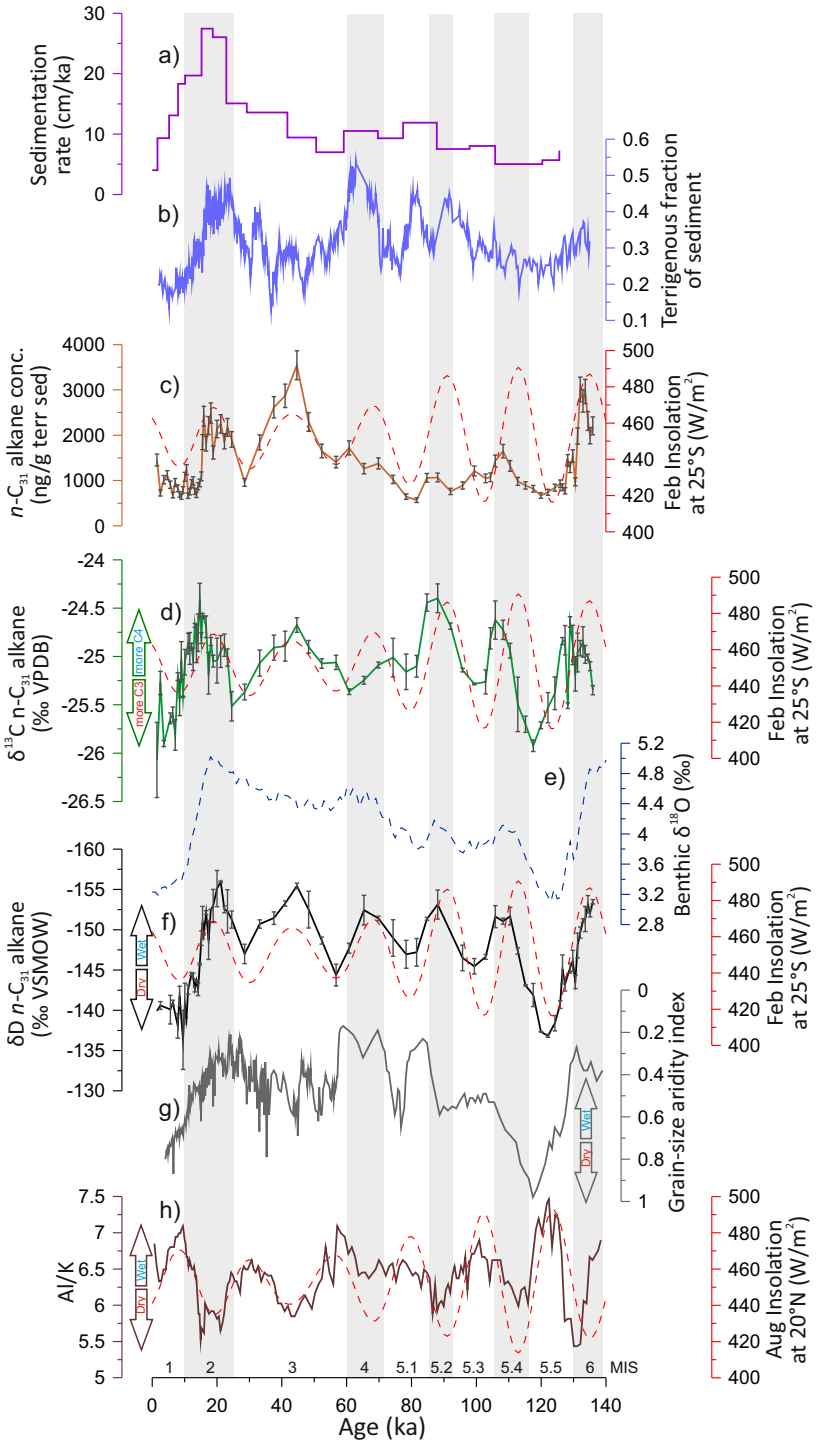
a)
b)
c)
d)
e)
f)
g)
h)
Sedimentation rate (cm/ka)
Terrigenous fraction of sediment
n-C31 alkane conc. (ng/g terr sed)
Feb Insolation at 25°S (W/m2)
δ13C n-C31 alkane (‰ VPDB)
more C4
more C3
δD n-C31 alkane (‰ VSMOW)
Benthic δ18O (‰)
Grain-size aridity index
Dry
Wet
Al/K
Aug Insolation at 20°N (W/m2)
1
2
3
4
5.1
5.2
5.3
5.4
5.5
6
MIS
Age (ka)